Int. J. Electrochem. Sci., 15 **(2020)** 11294 – 11305, doi: 10.20964/2020.11.60

International Journal of ELECTROCHEMICAL SCIENCE
www.electrochemsci.org

Short Communication

Preparation of Rod-shaped Bi_5O_7I as Bifunctional Material for Supercapacitors and Photcatalysts

Pei Wu[1,2,], Wenbin Xu[3], Xin Gu[1,2], Mingyuan Wang[1,2], Bingzhi Liu[4,*], Sarfaraz Khan[4]*

[1] School of Civil Engineering, Chang'an University, Xi'an 710061, China
[2] Key Laboratory of Water Supply & Sewage Engineering, Ministry of Housing and Urban-rural Development, Chang'an University, Xi'an 710061, China
[3] 599 Chunhui Road, Honggutan New District, Nanchang Urban Planning & Design Institute, Nanchang 330038, Jiangxi, China
[4] School of Civil and Transportation Engineering, Guangdong University of Technology, Guangzhou 510006, Guangdong, China
[*]E-mail: peterwoody@163.com (Pei Wu) and 15922887515@163.com (Bingzhi Liu).

Received: 20 July 2020 / *Accepted:* 16 September 2020 / *Published:* 30 September 2020

The preparation of new functional materials is one of the most effective, yet difficult methods for solving both energy shortage and environmental pollution problems. Bismuth iodide series oxides have been increasingly studied and favored in the field of supercapacitors and photocatalysts due to their unique morphological characteristics and excellent electrochemical performance. In this study, 3D rod-shaped Bi_5O_7I rich in bismuth and oxygen was synthesized from BiOI by adjusting the pH. A variety of advanced characterization techniques were used to systematically study the chemical composition, structural characteristics, surface properties, morphological characteristics and electrochemical and photocatalytic performance. Results showed that flaky BiOI and 3D rod-shaped Bi_5O_7I were successfully prepared with good crystal structure and high phase purity. The electrochemical impedance spectroscopy (EIS) of rod-shaped Bi_5O_7I were lower than BiOI because Bi^{3+} could easily migrate in Bi_5O_7I to reach a higher specific capacitance value (363 F/g). The high capacitance retention rate (72.9%) of rod-shaped Bi_5O_7I electrode indicated its high-rate capability. In addition, because of the large forbidden band width and suitable conduction and valence band positions of Bi_5O_7I, an increased number of holes could be generated under visible light radiation while the recombination of electrons and holes could be effectively hindered, thereby improving the photocatalytic performance. Carbamazepine (CBZ) anticonvulsant wastewater was degraded efficiently with a degradation rate of 97.1%, and K (degradation rate constant) of 0.021/min. In addition, recycling performance was also satisfactory, and the degradation efficiency of CBZ still remained above 85% after 6 cycles. This study provides a new way to develop new efficient supercapacitor electrodes for degrading organic pollutants in the environment.

Keywords: Supercapacitor; Photocatalysis; Bi_5O_7I; BiOI; Carbamazepine; Degradation

1. INTRODUCTION

With the rapid development of social economy, people gradually realize two main problems facing them today, namely, energy shortage and environmental pollution [1], therefore, scientists are committed to solving these problems through scientific research and innovation. As a sustainable and green water treatment technology, semiconductor photocatalysis efficiently degrades organic pollutants using sunlight, greatly reducing environmental pollution [2,3]. Therefore, photocatalysts that efficient activity should be developed to decompose and remove water pollution. In addition, people's social and economic development in the future will be significantly affected by the depletion of fossil fuel resources. Therefore, it is crucial to develop alternative energy [4]. The growing demand for portable power storage equipment has also become a great concern. Therefore, the great challenge for scientists and industry is to find solutions for environmental pollution and prepare efficient renewable energy storage equipment. Due to their fast discharge capability, safe operation, environmental remediation ability, recyclability and good stability, supercapacitor equipment has become a substitute product for lithium batteries, which has made a large impact on the scientific research community [5,6]. As a member of the bismuth oxyhalide family, BiOI is widely used in the field of environmental remediation owing to its excellent visible light absorption rate and excellent degradation ability to various forms of pollutants [7-9]. Moreover, it has also used to prepare electrode materials for energy conversion and supercapacitors due to the variable valence of Bi in BiOI.

However, in regard to BiOI, the combination of electrons and holes is greatly enhanced by the poor separation efficiency by photogenerated electron holes during excited electron migration [10]. In addition, due to the specific energy band position, the narrow band gap value is between 1.7 and 1.9 eV, its poor catalytic capacity has also become a major problem. Thus, a bismuth and oxygen enrichment strategy established by researchers is to adjust the energy band structure of BiOI [11,12], which not only introduces oxygen vacancies on the surface of BiOI to change the electron orbital structure for hindering the recombination of photogenerated electrons and holes, but also provides additional locations for adsorbing pollutants in electrochemical and photocatalytic processes [13]. Therefore, bismuth and oxygen-rich BiOI with built-in oxygen vacancies is expected to achieve excellent photocatalysis and supercapacitor performance [14]. Compared with BiOI, Bi_5O_7I exhibits high photocatalytic performance because of its powerful oxidation and reduction capabilities, and good catalytic performance due to a well-matched energy band position, which is widely used to degrade pollutants [15]. However, so far, there have been very few reports on the application of Bi_5O_7I for researching supercapacitors.

Wu et al has synthesized Bi_5O_7I with two-dimensional (2D) sheet, and it has good performance as a supercapacitor and shows excellent photocatalytic performance on Rhodamine B (RhB) and 4-chlorophenol (4-CP) degradation [16]. However, the 2D sheet shaped Bi_5O_7I encountered a bottleneck in improving the capacitance and photodegradation performance. The main reason is that the 2D sheet shaped Bi_5O_7I is exposed by few high-energy crystal surface, which has poor light utilization and reflection and large resistance to the free migration of the generated holes and of electrons. Thus, it is not conducive to the improvement of capacitance and catalytic performance. The 2D sheet shaped Bi_5O_7I is prone to interlayer stacking, the exposed high-energy crystal surfaces are easy to be blocked,

and the utilization of light decreases rapidly. The generated electrons and holes energy is easy to be weakened between stacked layers. As a result, it is not favorable for the free migration of Bi^{3+}. In addition, the overlapped Bi_5O_7I has small porosity and low specific surface area, poor storage electron performance, weak adsorption ability, and undesirable degradation performance. Therefore, it is necessary to strengthen the supercapacitor and photocatalysis performance of Bi_5O_7I by changing its spatial morphology rather than the composition. According to relevant research reports, the three-dimensional (3D) rod-shaped semiconductor materials generated by morphology control technology have excellent photoelectric and electrical properties [17]. It is mainly due to the fact that 3D rod-shaped semiconductors expose multiple high-energy crystal surfaces, multiply the light utilization, generate higher electrons and holes efficiency, and improve the degradation performance of pollutants. The constraint and resistance force for the free electron transfer is small, which also help to improve its electrical performance. 3D rod-shaped materials have less interference with each other, less space stacking, easier separation of the photogenerated electrons and holes, relatively longer degradation time for pollutants, and therefore those 3D rod-shaped materials possess obvious photocatalytic degradation performance. Besides, the specific surface area of the 3D rod-shaped semiconductor materials is large, and the more space between them is easy to generate, which is effective to the storage of electrons and can significantly improve their capacitance performance. Murakami et al synthesized 3D rod-shaped TiO_2, and confirmed that its {001} high-energy crystal surface had excellent photoelectric properties, and the degradation performance of RhB and 4-CP was very desirable [18]. Ye et al prepared the 3D rod-shaped MnO_2 semiconductor material, and it was confirmed to have excellent electrical properties with a high CF of 398 F/G at a high current of 50 mA, a low EIS of Ω $0.21 \cdot cm^2$ and a long cycle- life and high coulombic efficiency after charging and discharging 1000 cycles [19]. 3D-Shaped MnO_2 was regarded as an outstanding supercapacitor material. Compared with the 2D sheet Bi_5O_7I, if the 3D rod-shaped Bi_5O_7I can be synthesized by shape control technology, its photoelectric performance will be tremendously improved, which is of great significance. Therefore, based on BiOI, 3D-rod shaped Bi_5O_7I is supposed to be prepared in this study for the degradation of pollutants and the preparation of supercapacitors.

In this work, 3D rod-shaped Bi_5O_7I is synthesized from BiOI by changing the pH. Bi_5O_7I can be used as the electrode material of supercapacitors to provide a high specific capacitance value, where it can achieve a high specific capacitance value of 363 F/g, a low resistance value and long-term cycling stability. Additionally, Bi_5O_7I can still reach 72.9% of its initial specific capacitance after 6000 cycles. The prepared sample can be used as a photocatalyst to catalyze and degrade the antibiotic carbamazepine (CBZ) in organic wastewater under visible light. The degradation rate of CBZ by Bi_5O_7I is 97.1% within 2 hours, while that of BiOI is only 37.7%. The catalytic degradation rate of Bi_5O_7I can still be maintained above 85% after recycling 6 times. Finally, it has been observed that holes, and not hydroxyl radicals, are the main driving force for the degradation of CBZ by Bi_5O_7I.

2. EXPERIMENTAL PART

2.1 Materials

In this experiment, bismuth nitrate pentahydrate（III）($Bi(NO_3)_3·5H_2O$), potassium iodide (KI), and glacial acetic acid (HAc) were purchased from Shanghai Haiqu Chemical Co., Ltd. (Shanghai, China). Carbamazepine (CBZ) was provided by Xi'an Kangnuo Chemical Co., Ltd. (Xi'an, China) Hydrochloric acid and NaOH were from Wuhan Jinglong Chemical Co., Ltd. (Wuhan, China). Triethanolamine (TEOA) and tert-butanol (t-BuOH) were purchased from Jinan Kaijun Chemical Co., Ltd. (Jinan, China) and Shandong Yinglang Chemical Co., Ltd. (Jinan, China), respectively. Deionized water was used throughout the experiment.

2.2 Sample preparation

The preparation of BiOI was as follows. 0.02 mol $Bi(NO_3)_3·5H_2O$ and 18 ml glacial acetic acid (HAc) were dissolved in 200 ml deionized water. Then 0.02 mol KI was dissolved in 200 mL deionized water, and this solution was dropwise added to the first solution containing Bi^{3+}. The mixed solution was magnetically stirred for 40 min. The solid product was collected by centrifuging the above mixed suspension, and BiOI was obtained after multiple washing and vacuum drying at 80 ℃. The synthesis steps of Bi_5O_7I were as follows. 2.4 g NaOH was slowly added to 150 mL 2:1 (V/V) ethanol-water mixture. 2.0 g BiOI was added slowly after vigorous stirring at room temperature. A solid precipitate was formed after 50 min of magnetic stirring. Bi_5O_7I was obtained after washing for 5 times with 0.001 mol/L HCl and vacuum drying at 80 ℃.

2.3 Characterization

X-ray diffraction (XRD) of the product was obtained on an X-ray diffractometer (DMAX/2C, Rigaku, Japan) with Cu Kα radiation (λ=0.15418 nm). The micromorphological structure was characterized by scanning electron microscopy (SEM, REGULUS8230, Hitachi, Japan). The selected area electron diffraction (SEAD) and lattice characteristics of the products were observed using transmission electron microscopy (HR-TEM JOEL 2200 model). UV-Vis diffuse reflectance spectrum was recorded on UV-Vis (JASCO V-750) spectrophotometer at room temperature. The photoluminescence (PL) of the products were obtained using an F-7000 photoluminescence analyzer, and the electrochemical measurement value was recorded by a CHI-660B electrochemical workstation. The as-prepared samples of BiOI and Bi_5O_7I were regarded as the working electrodes, platinum and Ag/AgCl (filled with KCl) were regarded as counter electrodes and reference electrodes, respectively. The performance of the supercapacitor was detected using an electrolyte solution of 2.0 M KOH, while 0.5 M Na_2SO_4 was selected as the electrolyte for photocurrent study.

2.4 Photocatalytic performance

A certain amount of photocatalyst (BiOI and Bi_5O_7I) and a certain volume of CBZ (10 mg/L) simulated organic wastewater were added to a quartz tube with successive magnetic stirring. The solution was stirred by an agitator under dark conditions for 30 min to achieve absorbance/desorption equilibrium between the photocatalyst and target pollutant CBZ, and then its absorbance was measured (λ=285 nm). Photocatalysis experiments were carried out in a photoreaction apparatus (BL-GHX-V, Shanghai Bilang Instrument Co., Ltd., Shanghai, China). At regular intervals, 5 mL of CBZ solution was transferred, centrifuged and filtered. The CBZ concentration was determined by ultrahigh performance liquid chromatography (UPLC, Waters 2010), and a Symmetry C18 column (4.6 mm×250 mm, 5 μm, Waters) was used. The mobile phase was acetonitrile: water = 60:40, the detection wavelength was 286 nm, and the flow rate was 1 ml/min. The formula for CBZ degradation rate was as follows:

$$\text{Degradation rate} = (C_0 - C_t)/C_0 \times 100\% \quad (1)$$

Where C_0 is the absorbance of the CBZ solution after reaching the adsorption-desorption equilibrium, and C_t is the absorbance of the CBZ solution after being photocatalyzed for time of t.

3. RESULTS AND DISCUSSION

3.1 XRD and XPS analyses

XRD and XPS was conducted to determine the purity and crystallinity of the synthesized samples. The XRD patterns are shown in Fig. 1(a).

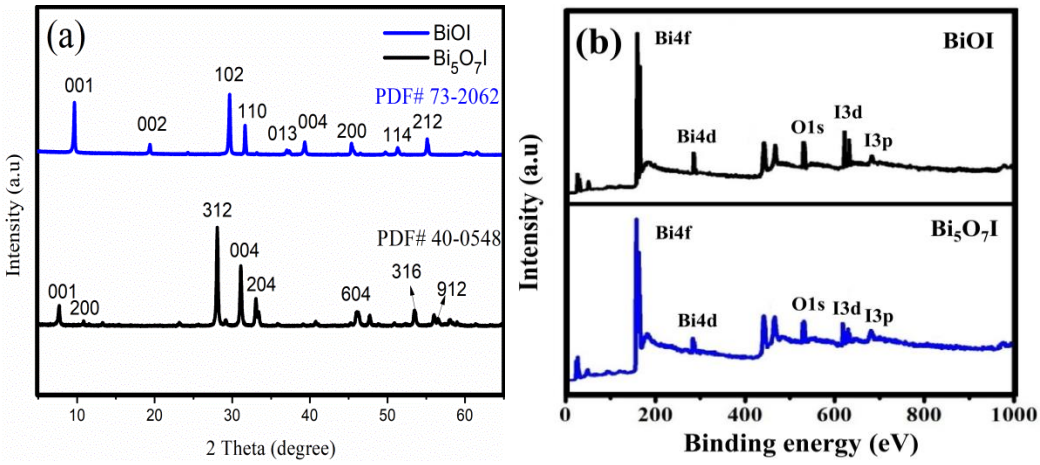

Figure 1. XRD (a) and XPS (b) patterns of BiOI and Bi_5O_7I.

The characteristic diffraction peaks of BiOI were found at 9.8° (001), 19.3° (002), 29.6° (102), 31.9° (110), 37.2° (013), 39.5° (004), 45.5° (200), 51.5° (114) and 55.4° (212), corresponding to the tetragonal structure of BiOI (JCPDS card No.10-0445). The characteristic diffraction peaks of Bi_5O_7I were located at 7.8° (001), 10.9° (200), 28.2° (312), 31.2° (004), 33.3° (204), 46.4° (604)、53.7° (316) and 56.2° (912)), corresponding to the orthorhombic structure of Bi_5O_7I (JCPDS card No.40-

0548). No characteristic peaks of any other impurity phase were observed in the pattern, which indicated very high purity and crystallinity of the synthesized samples [20]. Therefore, the synthesis of Bi_5O_7I from BiOI by adjusting the pH could be confirmed. In addition, as shown in Fig. 1(b), the results of XPS full spectrum for BiOI and Bi_5O_7I indicated that BiOI and Bi_5O_7I all contained Bi, O and I. No new elements or stray peaks were detected and observed, which verified the high purity of the products.

3.2 SEM analysis

The surface morphological characteristics of BiOI and Bi_5O_7I analysis are shown in Fig 2. Clearly, there was an evident morphology difference between BiOI and Bi_5O_7I.

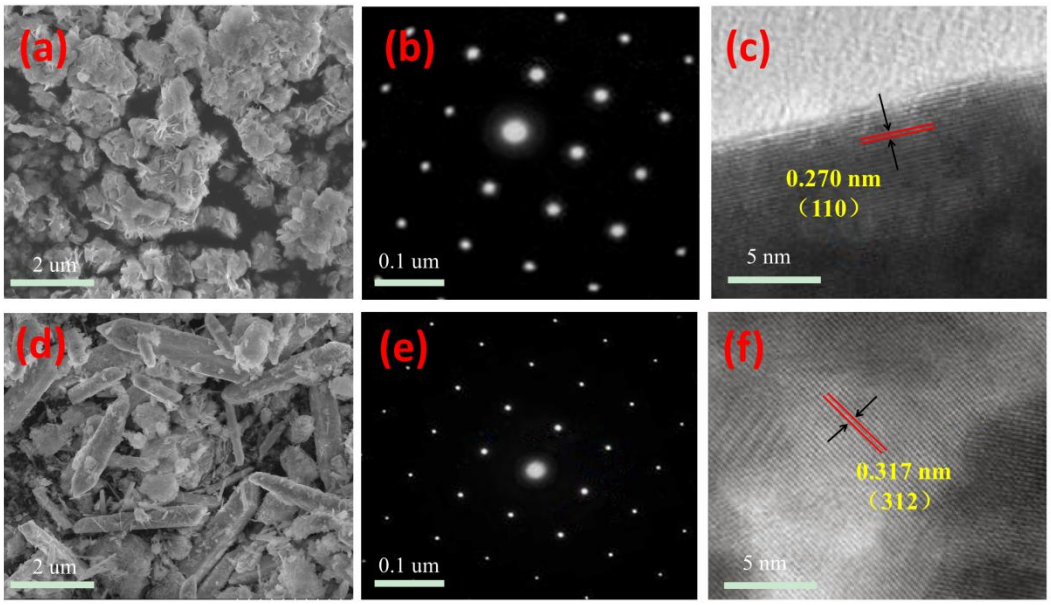

Figure 2. SEM (a, d), SAED (b, e) and HR-TEM (c, f) images of BiOI and Bi_5O_7I.

BiOI (Fig. 2a) presented a lamellar structure, with petal shapes stacked by many nanosheets, and Bi_5O_7I clearly presented a rod-shaped structure, which suggested the large influence pH had on the morphology of Bi_5O_7I. As shown in Fig. 2b and e, the SAED characteristics and lattice fringes of BiOI and Bi_5O_7I were analyzed using HR-TEM. The clear electron diffraction spots in BiOI and Bi_5O_7I indicated their high crystallinity, which was consistent with the XRD and XPS results. The continuous lattice fringes were 0.270 and 0.317 nm, which matched the atomic planes (110) and (312) of BiOI and Bi_5O_7I, respectively. Compared to the 2D sheet morphology of BiOI, the 3D rod-shaped structure of Bi_5O_7I semiconductor could effectively create and use electrons and holes. Thus, the rod-shaped structure significantly increased the light reflection and utilization efficiency by making better use of characteristic high-energy crystal surface to improve the photocatalytic performance [21]. In addition, the surface of the rod-shaped Bi_5O_7I could expose more active sites and had a larger specific surface

area to facilitate the migration of active conductive ions, thus the storage capacity and ion mobility in the electrochemical reaction could be improved to obtain better supercapacitor performance [22].

3.3 Supercapacitor performance analysis

As shown in Fig. 3, the supercapacitor properties were evaluated and researched in detail by a constant current charge/discharge (GCD) study with a voltage range of 0-1.0 V and a current density of 1.0-5.0 A/g.

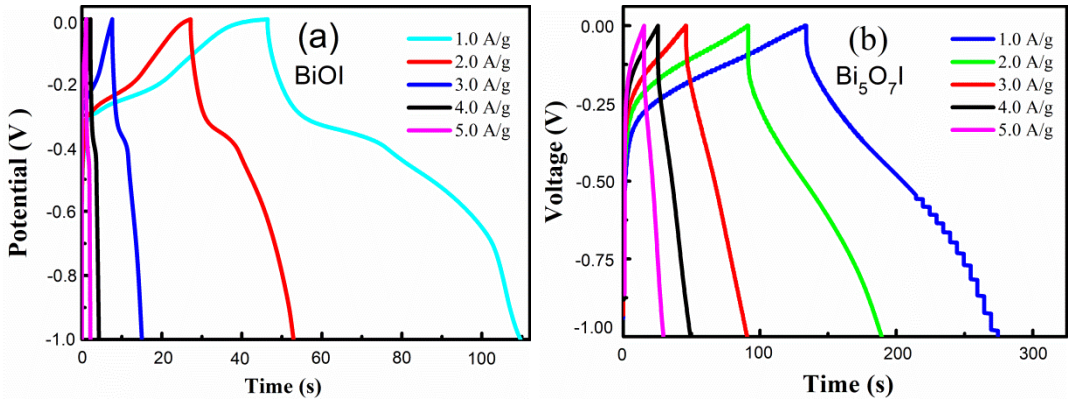

Figure 3. GCD curves of BiOI (a) and Bi_5O_7I (b) at the current density of 1-5A/g.

The GCD of BiOI and rod Bi_5O_7I exhibited a distinct divergent plateau trend, indicating typical pseudo-capacitance (Faraday process) properties. This result was mainly caused by the rapid charge transfer of Bi^{3+} ions on the electrode interface. According to the GCD results, at current densities of 1, 2, 3, 4 and 5 A/g, the specific capacitances (F/g) of BiOI electrodes were 103, 87, 53, 27 and 22 F/g, respectively, while the specific capacitances (F/g) of rod-shaped Bi_5O_7I were 363, 234, 201, 127 and 34 F/g, respectively. Compared with BiOI, rod-shaped Bi_5O_7I significantly improved specific capacitance, and had excellent capacitance performance. In addition, at higher current density, a steady decline in specific capacitance value of BiOI and rod-shaped Bi_5O_7I was clearly observed. This phenomenon manifested that the specific capacitance value decreased with the increase of current density [23]. At very low current densities, the hydroxide ions produced by the alkali moved very slowly and effectively interacted with the electrode materials, thereby promoting a strong redox reaction in the reversible process [24]. At the same time, after 6000 cycles, the rod-shaped Bi_5O_7I electrode had a better capacitance retention rate of 72.9%, indicating that the Bi_5O_7I electrode showed a high-rate capability.

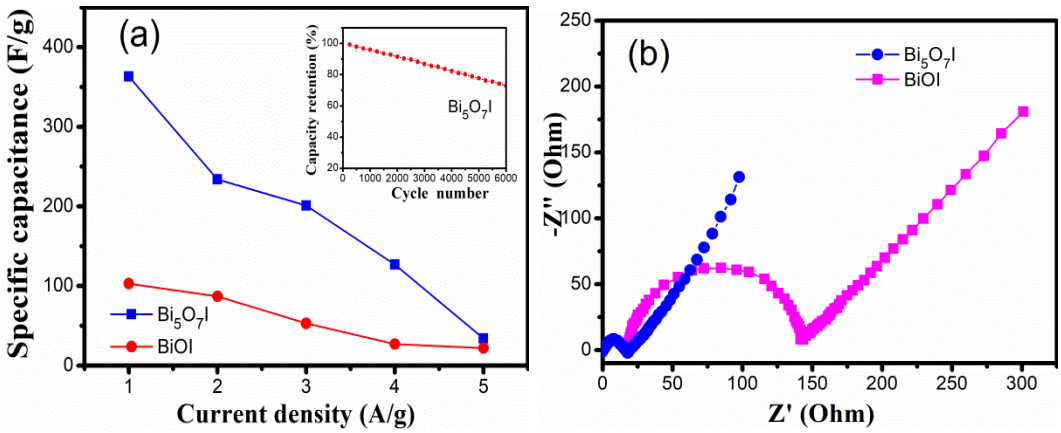

Figure 4. Capacitance values (a) and EIS (b) of BiOI and Bi_5O_7I.

Fig. 4(b) displays the electrochemical impedance spectroscopy (EIS) for BiOI and rod-shaped Bi_5O_7I from 100 kHz to 0.01 Hz. Nyquist plots with semicircle at high frequencies and slope at low frequencies were clearly observed. The resistance value of charge transfer resistance (Rct) of rod-shaped Bi_5O_7I electrode was lower than that of BiOI electrode. This result meant that the high specific capacitance was caused by high ionic conductivity and rapid electron transfer performance on the surface of the rod-shaped Bi_5O_7I electrode [25]. According to the GCD and EIS results discussed above, the excellent electrochemical performance of the Bi_5O_7I electrode should be attributed to its unique structural characteristics. The higher specific capacitance of the Bi_5O_7I electrode was caused by the environment rich in oxygen and Bi, table rod shape morphology and low resistance value [26]. In addition, the pure chemical composition and stable crystal structure of Bi_5O_7I also promoted the rapid transmission of electrons and shortened the transmission path of ions into the electrode during the reaction.

3.4 Photocatalytic analysis

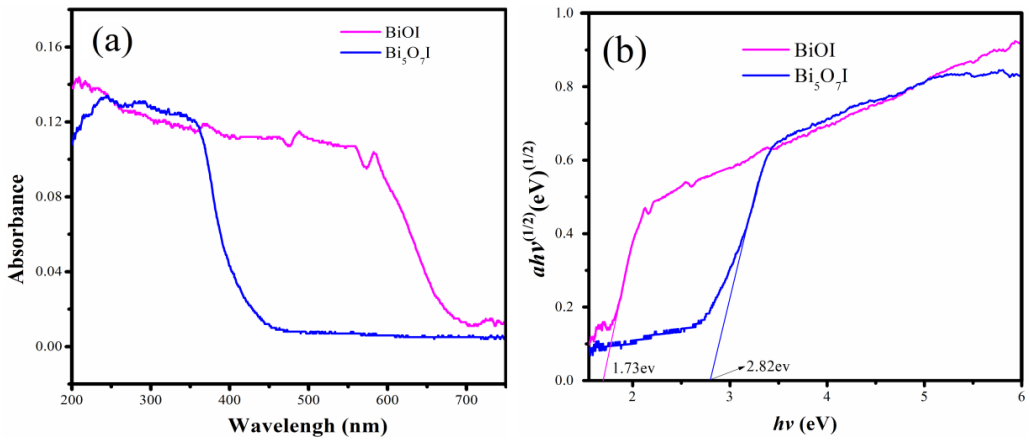

Figure 5. UV-Vis diffuse reflectance spectra (a) and Tauc (b) of BiOI and Bi_5O_7I.

As one of the key points of photocatalytic applications, the optical absorption characteristics of BiOI and rod-shaped Bi_5O_7I were studied through UV-Vis in Fig. 5.

The band gap energy of BiOI and rod-shaped Bi_5O_7I could be estimated from the intercept of the tangents to the plot of $(ahυ)^{1/2}$ versus energy ($hυ$). The obtained Eg values of BiOI and Bi_5O_7I were 1.79 and 2.82 eV, respectively. Compared with BiOI, the band gap of Bi_5O_7I increased, and its conduction and valence bands were more suitable. Under the visible light radiation, a large number of holes could be generated, and the combination of electrons and holes was effectively hindered, which improved the photocatalytic performance [27].

In Fig. 6(a), the PL of BiOI and Bi_5O_7I were obtained at an the excitation wavelength of 475 nm. Clearly, the PL strength of Bi_5O_7I was lower than that of BiOI, indicating that the photogenerated free charge carriers of Bi_5O_7I had a strong ability to transfer and separate, which contributed to the improvement in photocatalytic activity. In addition, Fig. 6(b) showed the analysis of the photocurrent response of BiOI and rod-shaped Bi_5O_7I. The photocurrent response of rod-shaped Bi_5O_7I was stronger than that of BiOI, the intensity was nearly 10 times that of BiOI, demonstrating that rod-shaped Bi_5O_7I facilitated the separation of electrons (e^-) and holes (h^+) to yield enough h^+ during the photodegradation process. With strong oxidation properties, these holes (h^+) could rapidly decompose organic pollutants rapidly and showed desirable photocatalytic performance [28].

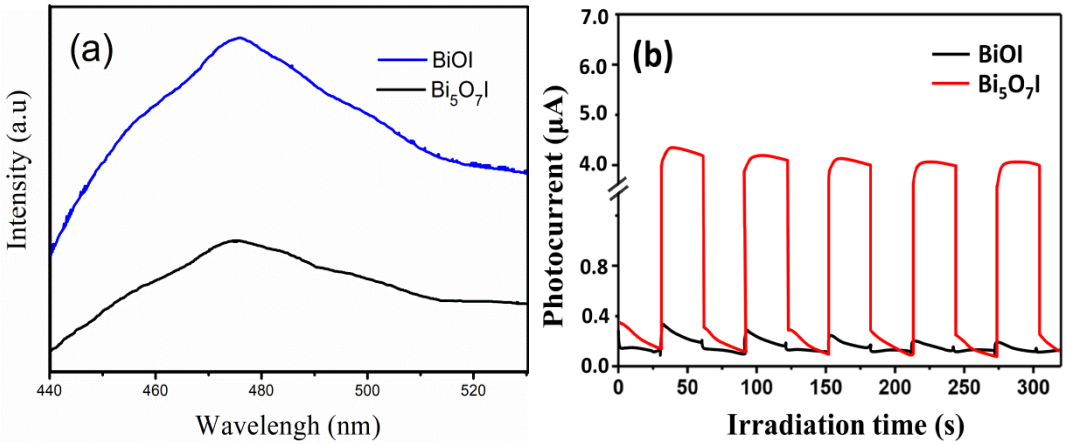

Figure 6. PL (a) and photoresponse (b) of BiOI and Bi_5O_7I samples.

The prepared BiOI and rod-shaped Bi_5O_7I were used to degrade CBZ antibiotic wastewater to evaluate its photocatalytic performance.

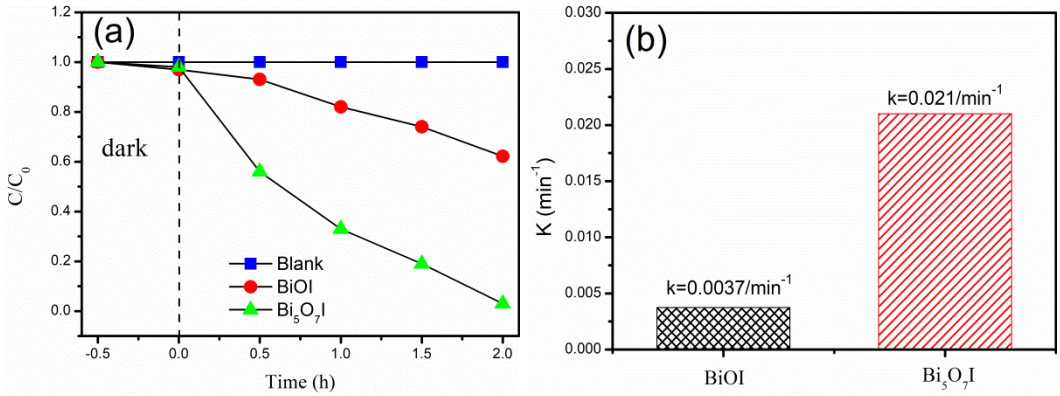

Figure 7. Photodegradation efficiency (a) and degradation rate (b) of CBZ at pH of 6.0 and dosadge of 40 mg/L.

In Fig. 7, after 30 min to adsorption-desorption equilibrium, the remaining concentration of CBZ gradually decreased with an increasing illumination time. However, the residual concentration of CBZ in the blank test did not change, indicating that the CBZ was degraded by the photocatalysis of BiOI and rod-shaped Bi_5O_7I. Compared with BiOI, rod-shaped Bi_5O_7I had an obvious CBZ removal effect and excellent photocatalytic performance. After 2 hours of light, the removal of CBZ by rod-shaped Bi_5O_7I reached 97.1%, while the removal of CBZ by BiOI was only 37.7%. The degradation of KBZ was significantly enhanced by the rod-shaped Bi_5O_7I. The degradation kinetics of CBZ was analyzed further (first-order kinetic model). After calculation, the k (degradation rate constant) of Bi_5O_7I was 0.021/min, which was much larger than 0.0037/min of BiOI. Thus, compared with BiOI, the rod-shaped Bi_5O_7I displayed excellent photocatalytic performance under the same experimental conditions. The rod-shaped Bi_5O_7I, which contained an abundance of oxygen vacancies and active Bi, greatly expanded the band width and produced appropriate conduction and valence bands. As a result, Bi_5O_7I facilitated the separation of electrons and holes, and slowed down their combination [29]. Holes with strong oxidizing properties could quickly destroy the organic structure of CBZ to further degrade and mineralize it.

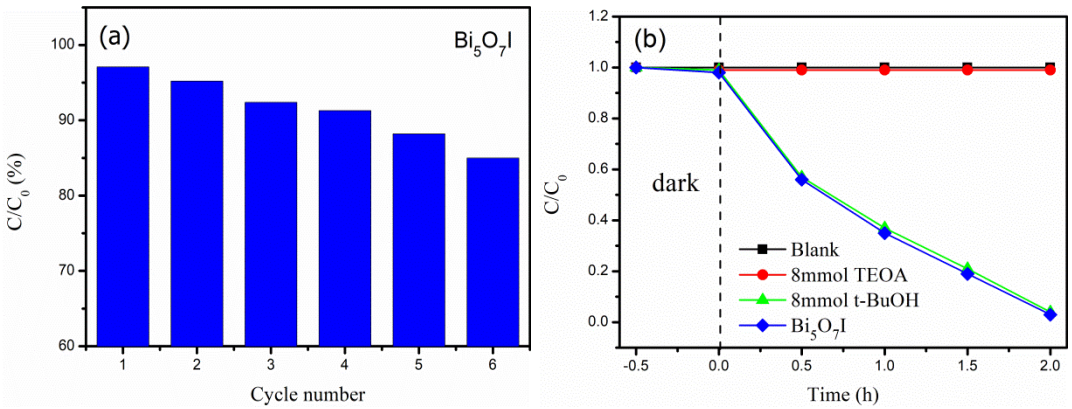

Figure 8. Recycling performance (a) at pH of 6.0 and dosadge of 40 mg/L and trapping experiments (b) of Bi_5O_7I.

As shown in Fig. 8(a), after repeated use of Bi_5O_7I 6 times, its photocatalytic performance decreased, but the photocatalytic efficiency toward CBZ remained above 85%. Therefore, the good recyclable performance of rod-shaped Bi_5O_7I has excellent potential for use in market applications.

The type of active catalytic substance should be detected to further explore the mechanism of the photocatalytic degradation of CBZ by rod-shaped Bi_5O_7I. As the most likely active sites for degrading CBZ, holes (h^+) and hydroxyl radicals (•OH) were analyzed by trapping experiments that used triethanolamine (TEOA) as h^+ scavenger and t-BuOH as •HO scavenger. The CBZ degradation suddenly stopped and almost approached the blank value after the addition of TEOA, proving that h^+ was the main reason for the degradation of CBZ by rod-shaped Bi_5O_7I. At the same time, the degradation of CBZ was almost unaffected after adding t-BuOH, proving that •OH was not the main reason for the degradation of CBZ in the photocatalytic process. Based on the above analysis, we believe that under the irradiation of visible light, a large number of holes (h^+) were generated from rod-shaped Bi_5O_7I to effectively degrade and remove CBZ. Previous studies also had similar findings [30].

4. CONCLUSION

In this study, rod-shaped Bi_5O_7I was successfully synthesized from BiOI by simply adjusting pH value. The high phase purity and the good crystal structure of BiOI and Bi_5O_7I were confirmed by XRD, XPS and SEAD analyses. BiOI presented a clear lamellar petal-shaped structure and Bi_5O_7I showed a rod-shaped morphology. According to the electrochemical results, the electrical properties of rod-shaped Bi_5O_7I was excellent and clearly better than those of BiOI. The rod-shaped Bi_5O_7I featured a relatively low Rct, large specific capacitance (363 F/g) and excellent electric storage performance. After 6,000 charge/discharge cycles, the Bi_5O_7I electrode could still reach 72.9% of capacitance. Therefore, as a potential supercapacitor material, Bi_5O_7I electrode presented potential value for use in commercial applications. In addition, the rod-shaped Bi_5O_7I exhibited a high removal rate of CBZ (97.1%) and a high degradation rate constant (k=0.021/min). The recycling performance of Bi_5O_7I was better, and its removal efficiency of CBZ remained above 85% after being recycled 6 times. During the catalytic degradation of CBZ, rod-shaped Bi_5O_7I produced a large number of active holes (h^+) to efficiently degrade and remove CBZ. This synthesized rod-shaped Bi_5O_7I rich in bismuth and oxygen is expected to be used in the treatment of organic wastewater and in the preparation of advanced energy storage devices in the near future.

ACKNOWLEDGEMENT
The authors are grateful for the financial support provided by the Science and Technology Project of Shaanxi Province, China (Grant No.:2018JQ5143).

References

1. R. Hemmati, H. Saboori and M.A. Jirdehi, *Renew Energ*., 97 (2016) 636.
2. P.K.J. Robertson, *J Clean Prod*., 4 (2016) 203.

3. Z. Jiang, L. Feng, J. Zhu, X. Li, Y. Chen and K. Sarfaraz, *Ceram Int*., 46 (2020) 19084.
4. A. Hezam, K. Namratha, Q.A. Drmosh, B.N. Chandrashekar, G.K. Jayaprakash, C. Cheng, S.S. Swamy and K. Byrappa, *Ceram Int*., 44 (2018) 7202.
5. Z. Gao, J. Fang, Y. Zhang and D. Sun, *J Mod Power Syst Cle*., 2 (2014) 181.
6. R. Yuan, H. Wang, M. Sun, K. Damodaran and T. Kowalewski, *ACS Appl Nano Mater*., 2 (2019) 2467.
7. D. Chen, J. Yang, Y. Zhu, Y. Zhang and Y. Zhu, *Appl Catal B-Environ*., 233 (2018) 202.
8. S. Park, N.M. Shinde, P.V. Shinde, D. Lee, J.M. Yun and K.H. Kim, *Dalton T*., 49 (2020) 774.
9. F. Dong, Y. Sun, M. Fu, Z. Wu and S.C. Lee, *J Hazard Mater*., 219 (2012) 26.
10. G. Dai, J. Yu and G. Liu, *J Phys Chem C*., 115 (2011) 7339.
11. C. Liu, H. Huang, X. Du, T. Zhang and Y. Zhang, *J Phys Chem C*., 119 (2015) 17156.
12. X. Xiao, C. Xing, G. He, X. Zuo, J. Nan and L. Wang, *Appl Catal B-Environ*., 148 (2014) 154.
13. R. He, S. Cao, J. Yu and Y. Yang, *Catal Today*., 264 (2016) 221.
14. V. Renuga, C.N. Mohan and A. Manikandan. *Materials Research Bulletin*., 98 (2018) 265.
15. S. Sun, W. Wang, L. Zhang, L. Zhou, W. Yin and M. Shang, *Environ Sci Technol*., 43 (2009) 2005.
16. P. Wu, L. Feng, Y. Liang, X. Zhang, X. Li, S. Tian, H. Hu, G. Yin and S. khan, *J Mater Sci-Mater El*., 31 (2020) 538.
17. M. Thamima, and S. Karuppuchamy, *J Mater Sci-Mater El*., 27 (2016) 458.
18. .Y. Murakami, T. Kamegawa, Y. Kobori and T. Tachikawa, *Nanoscale.*, 12 (2020) 6420.
19. Y.Chen Ye, M. Zhang and Z. Shi, *J Electrochem Soc*., 152 (2005) 1272.
20. Y. Yu, G. Chen, X. Wang, D. Jia, P. Tang and C. Lv, *Rsc Adv*., 5 (2015) 74174
21. N. Roy, Y. Sohn and D. Pradhan, *Acs Nano*., 7 (2013) 2532.
22. D. Pocaznoi, B. Erable, M.L. Delia and A. Bergel, *Energ Environ Sci*., 5 (2012) 5287.
23. J. Han, L.L. Zhang, S. Lee, J. Oh, K.S. Lee, J.R. Potts, J. Ji, X. Zhao, R.S. Ruoff and S.J. Park, *Acs Nano*., 7 (2013) 19.
24. C. Ye, Z.M. Lin and S.Z. Hui, *J Electrochem Soc*., 152 (2005) 1272.
25. L.I. Li-Min, E.H. Liu,L.I. Jian, Y.J. Yang and X.X. Xiang, *Acta Phys-Chim Sin*., 26 (2010) 1521.
26. S.V. Kumar, N.M. Huang, N. Yusoff and H.N. Lim, *Mater Lett*., 93 (2013) 411.
27. B. Lu, C. Zhu, Z. Zhang, W. Lan and E. Xie, *J Mater Chem*., 22 (2011) 1375.
28. Y. Li, F. Yang and Y. Yu, *Appl Surf Sci*., 358 (2015) 449.
29. J. Guo, Z. Gan, J. Lu, J. Xi, Y. Wan, L. Le, H. Liu, J. Shi and R. Xiong, *J Appl Phys*., 114 (2013) 37.
30. Y. Fu, H. Chen, X. Sun, and X. Wang, *Appl Catal B-Environ*., 111 (2012) 280.